Frontiers of Information Technology & Electronic Engineering
www.jzus.zju.edu.cn; engineering.cae.cn; www.springerlink.com
ISSN 2095-9184 (print); ISSN 2095-9230 (online)
E-mail: jzus@zju.edu.cn

Correspondence:

Monopulse transmitarray antenna fed by aperture-coupled microstrip structure*

Na KOU[1,2,3], Shixing YU‡[1,2,3], Zhao DING[1,2,3], Zhengping ZHANG[1,2,3]

[1]*College of Big Data and Information Engineering, Guizhou University, Guiyang 550025, China*

[2]*Key Laboratory of Micro-Nano-Electronics and Software Technology of Guizhou Province, Guiyang 550025, China*

[3]*Engineering Research Center of Power Semiconductor Device Reliability of the Ministry of Education, Guiyang 550025, China*

E-mail: nkou@gzu.edu.cn; sxyu1@gzu.edu.cn; zding@gzu.edu.cn; zpzhang@gzu.edu.cn

Received Oct. 14, 2020; Revision accepted May 26, 2021; Crosschecked Dec. 21, 2021

https://doi.org/10.1631/FITEE.2000547

An X-band monopulse antenna based on transmitarray with light-weight and low-cost features is designed, fabricated, and measured. The proposed antenna is composed of a transmitarray lens, a feed source which combines aperture-coupled microstrip antennas, and a sum-difference (SUM-DIFF) comparator. According to simulation and measurement results of the transmitarray based monopulse antenna, gain of sum beam reaches 21.5 dBi. The sidelobe level is below −13.4 dB, and the cross polarization level is below −20 dB. In addition, the gain ratios between the sum beam and difference beam in E-plane and H-plane are 5.6 dB and 4 dB, respectively. The transmitarray based monopulse antenna could be applied in low-cost SATCOM on the move (SOTM) system.

1 Introduction

Monopulse technique, also known as the simultaneous beam comparison method, is used mainly to measure the direction of arrival (DOA) (Sherman and Barton, 2011). Before the advent of monopulse technology, the method most widely used in radar direction finding was the lobe-switching technique (sequential lobing) (Lo, 1999). Compared with the sequential lobing method, the monopulse antenna can obtain information such as the pitch angle, azimuth angle, and distance of the target in a single pulse period (Vazquez-Roy et al., 2019). Due to the need for higher accuracy of angle measurement, the monopulse technique has been widely applied in SOTM missile guidance (Roy et al., 2019). When a monopulse system is working, multiple independent channels are adopted to receive signals reflected by targets at the same time. Then signals enter the comparator and finally the distance and angle information of targets can be obtained. There are three main types of monopulse antennas: lenses, reflectors, and arrays. A dielectric lens is generally a convex lens (Raman et al., 1998), which is difficult to manufacture due to its curved shape, high volume, and large mass. For common reflectors such as dish antennas, the feed and supporting structure are in front of the aperture, so a shielding effect will result in energy loss, sidelobe increase, and angle measurement error (Kou and Cheng, 2019). A more effective reflector is the Cassegrain antenna, which is more compact with dual reflectors (Zheng et al., 2016, 2017). However, the Cassegrain antenna has the problem of shielding effect caused by a secondary reflector and support

‡ Corresponding author

* Project supported by the National Natural Science Foundation of China (No. 61961006) and the Science and Technology Projects of Guizhou Province, China (No. QKHJC[2020]1Y257)

ORCID: Na KOU, https://orcid.org/0000-0002-8410-4485; Shixing YU, https://orcid.org/0000-0003-4335-7520

rods. With growing demand for low cost and lightweight monopulse antennas in modern radar and telecommunications systems, array antennas are increasingly applied in monopulse antennas due to their characteristics of high gain and easy control of the beam direction. A typical example is the waveguide slot array, which has the advantages of low loss, low sidelobe level, and no aperture shielding problem (Vosoogh et al., 2018). The microstrip has attracted much attention in monopulse antennas because of its advantages of low profile, simple structure, and low cost (Yu et al., 2009; Kumar and Kumar, 2018). However, monopulse microstrip array antennas usually have a complex feed network, which often makes them large and expensive. In addition, substrate integrated waveguides (SIWs) (Cao et al., 2017; Zhu et al., 2018; Liu et al., 2019; Yang et al., 2019) and leaky wave antennas (LWAs) (Poveda-García et al., 2019) have been applied in monopulse antennas, with good results. Recently, reflectarrays have been proposed for use in monopulse antennas, and have shown good performance (Zhao et al., 2017, 2018). As an alternative to reflectarrays, transmitarrays not only have the advantages of reflectarrays, but also have no shielding effect from the feeds. Di Palma et al. (2016) proposed a 400-element reconfigurable transmitarray antenna to synthesize monopulse radiation patterns. However, the sum and difference patterns generated by the reconfigurable transmitarray antenna, which is controlled electronically by switches instead of by a SUM-DIFF comparator, are in time division.

In this study, we propose an X-band monopulse transmitarray antenna fed by an integrated structure. The monopulse transmitarray antenna combines aperture-coupled microstrip antennas (ACMAs) and a SUM-DIFF comparator. A two-layered transmitarray element with patches of variable sizes is adopted in the design to obtain high gain. A prototype of the X-band monopulse transmitarray antenna has been designed, fabricated, and measured.

2 Feed antenna performance

The configuration of the X-band monopulse transmitarray antenna is shown in Fig. 1. It is composed of a transmitarray and a feed source which combines

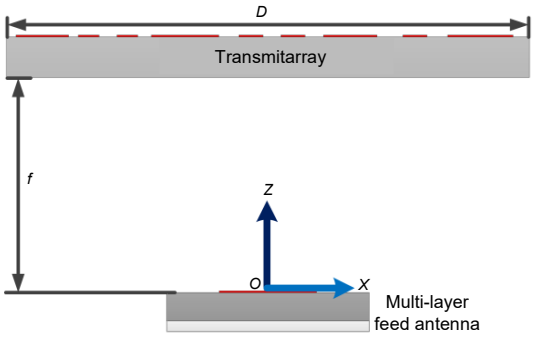

Fig. 1 Configuration of the X-band monopulse transmitarray antenna

ACMAs (Didouh et al., 2012) and a SUM-DIFF comparator. First, the performance of the ACMA unit cell is analyzed (Figs. 2a and 2b). The antenna operates at X-band and has relatively wide-angle radiation patterns. Next, to generate SUM-DIFF patterns, the SUM-DIFF comparator needs to be designed to feed the ACMA (Figs. 2c and 2d). The microstrip SUM-DIFF network consists of four 3-dB couplers and four 90° phase shift microstrip lines, all etched on 0.5-mm-thick RO4350B substrate (dielectric layer 1, from Rogers Corporation) with a dielectric constant of 3.48 and a loss tangent of 0.005. Four ACMA unit cells are placed at the terminal positions. Antenna element spacing is 19.99 mm along the *X* axis and 19.31 mm along the *Y* axis. SUM, DIFF1, and DIFF2 ports are linked to the monopulse feed for generation of sum and difference beams in the E-plane and H-plane. The dimension of the SUM-DIFF network is 72 mm×70 mm. The ACMA antennas are printed on a 2-mm-thick F4BM-2 substrate (dielectric layer 2, from Wangling Insulating Material Factory) with a dielectric constant of 2.2 and a loss tangent of 0.003.

Fig. 2 shows that the ACMA is integrated with the SUM-DIFF comparator, providing higher reliability compared to designs using discrete components. The fabricated prototype of the integrated feed source (Fig. 3) contains two layers: the SUM-DIFF network layer and the ACMA layer. Insertion losses from the SUM, DIFF1, and DIFF2 ports to the four ports of the antenna elements can be calculated (Fig. 4). Since the antenna elements are fed by an aperture-coupled microstrip structure, in practice the insertion losses cannot be measured. Hence, we deduce from full-wave simulation results that the loss of the SUM-DIFF comparator is acceptable. In addition, a performance

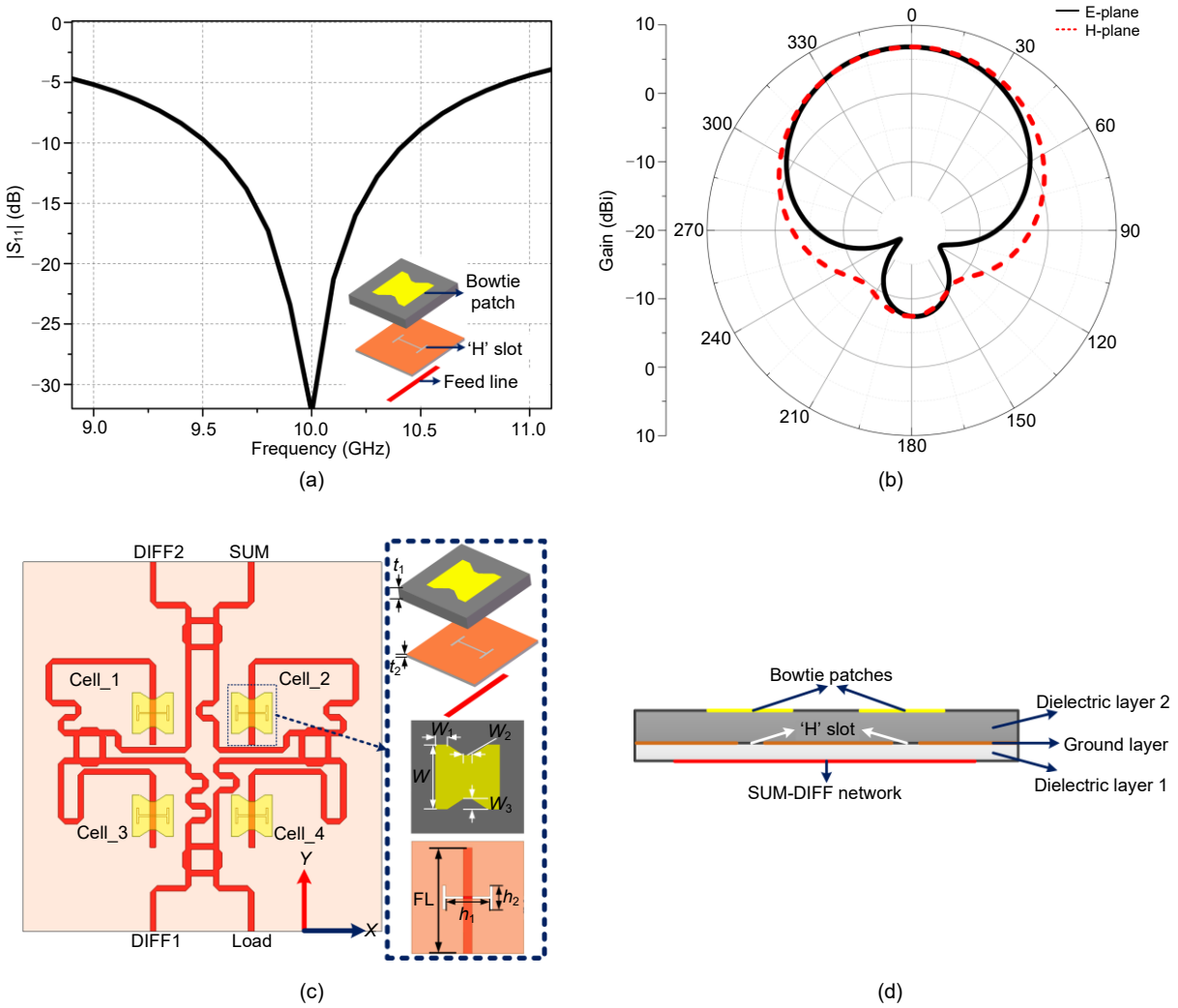

Fig. 2 $|S_{11}|$ (a) and radiation patterns (b) of the aperture-coupled microstrip antenna unit cell and top view (c) and side view (d) topology of the multi-layer feed antenna based on the aperture-coupled microstrip antenna
(W_1=1.5 mm, W_2=1 mm, W_3=1.3 mm, W=8 mm, h_1=5.5 mm, h_2=3 mm, FL=13.2 mm, t_1=2 mm, t_2=0.5 mm)

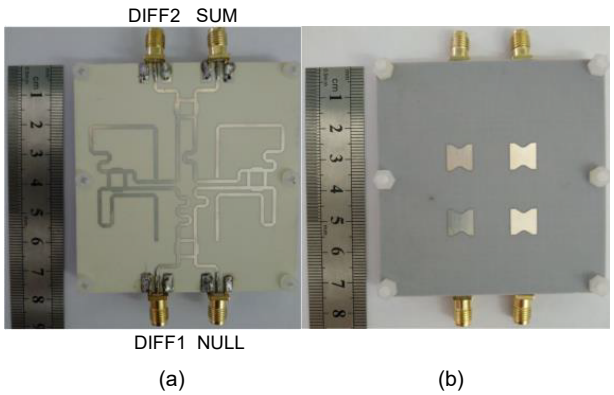

Fig. 3 Fabricated prototype of the multi-layer feed antenna: (a) SUM-DIFF network layer; (b) aperture-coupled microstrip antenna layer

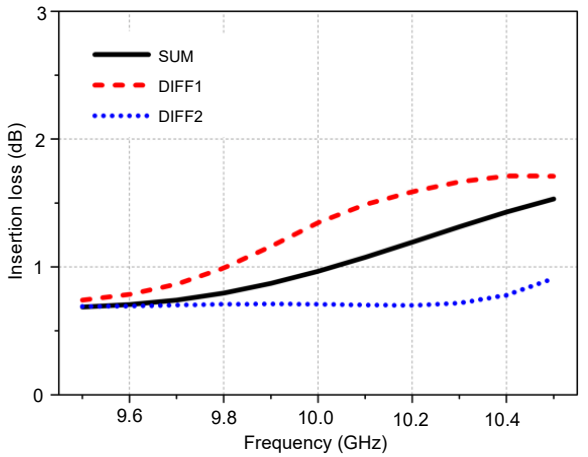

Fig. 4 Simulated insertion losses from the SUM, DIFF1, and DIFF2 ports to the four ports of the antenna elements

comparison between simulation and measurement of the multi-layer feed antenna is given in Fig. 5, from which we can see that the results show good agreement. The measured $|S_{11}|$'s of the SUM, DIFF1, and DIFF2 ports are all below −10 dB from 9.8 to 10.2 GHz. The measured isolations between two of the three channels are all below −15 dB from 9.6 to 10.4 GHz.

3 Transmitarray antenna design

To obtain phase regulation for the feed antenna using the transmitarray, a transmitted element with two layers of tightly bound substrates is proposed (Fig. 6a). The element is composed of three metallic layers printed on 2-mm-thick F4BM-2 substrates, with two identical square patches on two sides and one dual square-ring in the middle. The period of the transmitted element is 15 mm ($\lambda_0/2$ at the center operating frequency of 10 GHz). All the geometrical parameters of the dual square-ring (b, c, w_i, w_o) have a fixed linear relationship with the length of the square patch a (Table 1). Hence, to obtain a desired transmission phase shift, all the geometrical parameters of the metallic structures are adjusted when a is varying. At the same time, the insertion loss of the variable-size element needs to be as low as possible. Using master–slave boundary conditions with Floquet ports, the

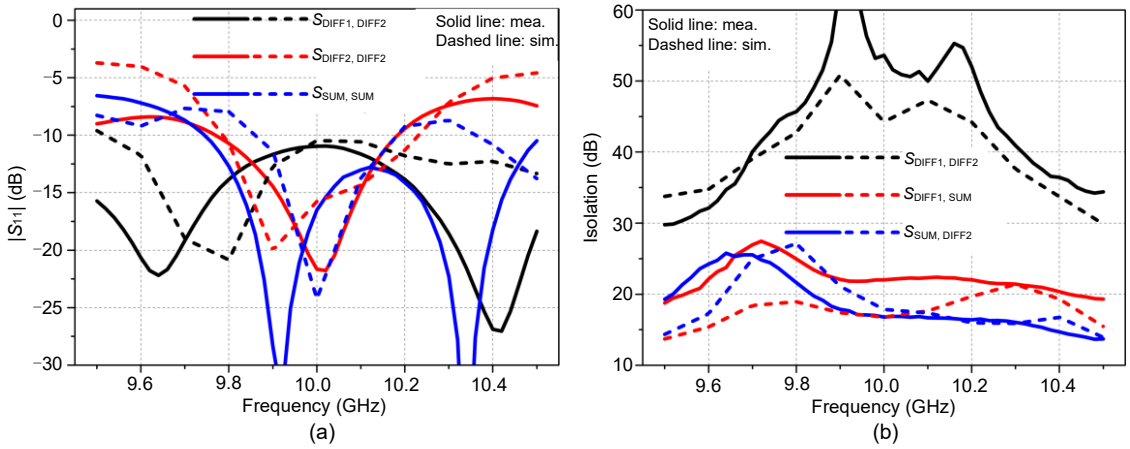

Fig. 5 Simulated (sim.) and measured (mea.) $|S_{11}|$ of sum port SUM, difference ports DIFF1 and DIFF2 of the multi-layer feed antenna (a) and simulated and measured isolation between the SUM, DIFF1, and DIFF2 ports (b)
References to color refer to the online version of this figure

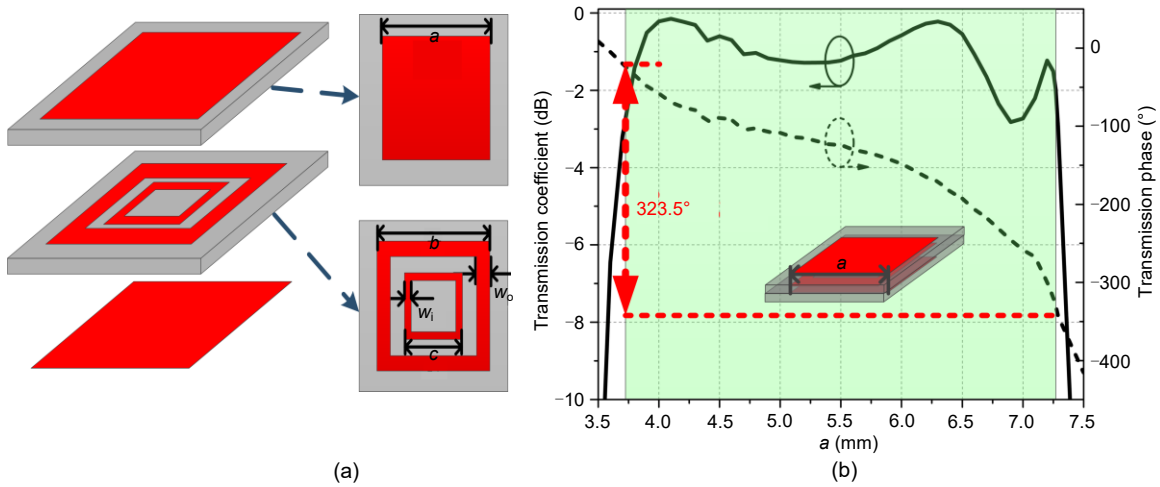

Fig. 6 Layout of the two-layered transmitted unit cell (a) and transmission coefficient and transmission phase of the transmitted element (b)

transmission coefficient (S_{21}) of the transmitted element is analyzed (Fig. 6b). When a is changed from 3.7 to 7.3 mm, the insertion loss remains less than 3 dB, with 1.1 dB on average, and the transmission phase ranges from −19.5° to −343°, covering 323.5°. Hence, the proposed transmitted unit cell can satisfy the phase modulation requirement of the transmitarray to obtain high gain.

Table 1 Geometrical parameters of the transmitted unit

a	b	c	w_o	w_i
3.7–7.3 mm	1.83a	0.82a	0.4a	0.24a

Fig. 7 shows the transmission coefficient and transmission phase of the transmitarray element at different oblique incidence angles for TE and TM polarized incident waves. The parameter θ is the elevation angle of the incident wave. As the oblique incident angle becomes larger, the feature of the transmission shows a very similar variation trend. In addition, when designing the transmitarray, elements with good angle and polarization stabilities are selected. The transmission coefficients of the transmitarray unit cells of different sizes as a function of frequency are analyzed (Fig. 8). As the operating frequency shifts, the available size range of the transmitarray unit cell changes. The effective phase shift range also varies as the frequency shifts.

The topology of the transmitarray-based monopulase antenna is shown in Fig. 9. The phase centers of the feed source and transmitarray lens are usually in a direct line with each other. To generate SUM-DIFF patterns, the phase shift distribution at position P can be calculated as follows (Abdelrahman et al., 2017):

$$\varphi_P = k_0 |OP| \pm 2n\pi, \tag{1}$$

where P is an arbitrary center point of a transmitarray element, O is the original point of the feed antenna, k_0 is the wave number in free space, and n represents an integer.

To determine the distance between the feed antenna and the transmitarray lens, the spillover, taper, and aperture efficiencies under different f/D ratios (focal length to diameter ratios) are analyzed (Fig. 10). When the f/D ratio increases, the spillover efficiency decreases, and the taper efficiency increases. The aperture efficiency reaches the peak at f/D=0.5. Under this condition, the spillover efficiency is 88% and the taper efficiency is 71.5%. In conclusion, f/D=0.5 is chosen to design the monopulse transmitarray antenna, which means that the feed source is placed 100 mm away from the transmitarray lens, since the diameter of the transmitarray is 200 mm.

In the measurement setup, the transmitarray and the multi-layer feed antenna with the SUM-DIFF network are mounted onto a plastic holder (Fig. 11). Two-dimensional far-field patterns in the XOZ plane (E-plane) and YOZ plane (H-plane) are measured in the range of ±60° at 10 GHz. Fig. 12 presents a comparison of sum patterns between simulation and measurement. From the results we can deduce that co-polarized sum beams in simulation and measurement agree

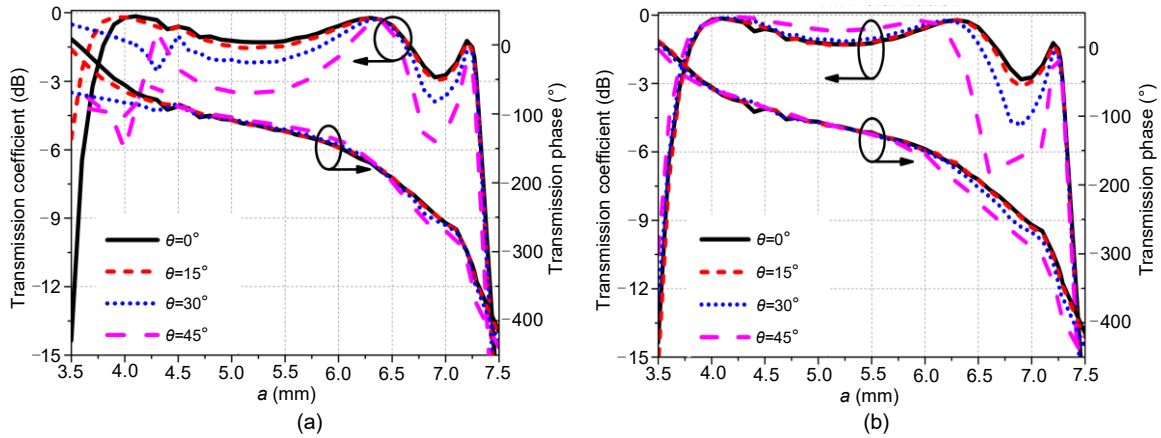

Fig. 7 Transmission coefficient and transmission phase of transmitarray unit cells under oblique incidences with TE polarization (a) and TM polarization (b)

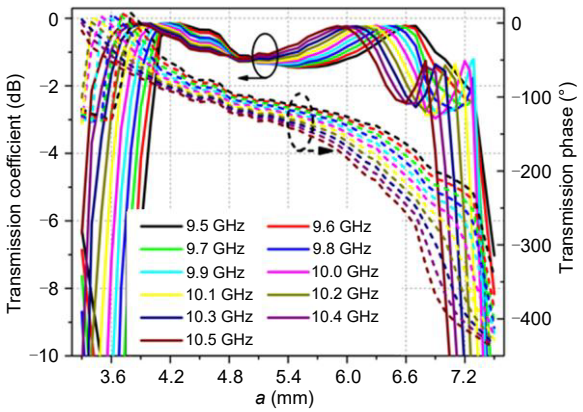

Fig. 8 Transmission coefficient and transmission phase of transmitarray unit cells of different sizes as a function of frequency

References to color refer to the online version of this figure

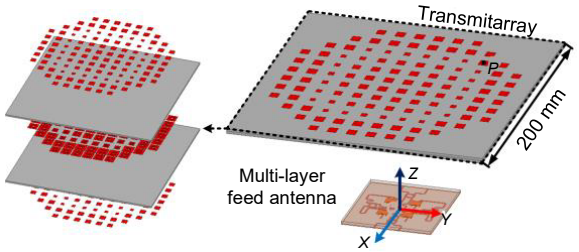

Fig. 9 Topology of the monopulse transmitarray antenna

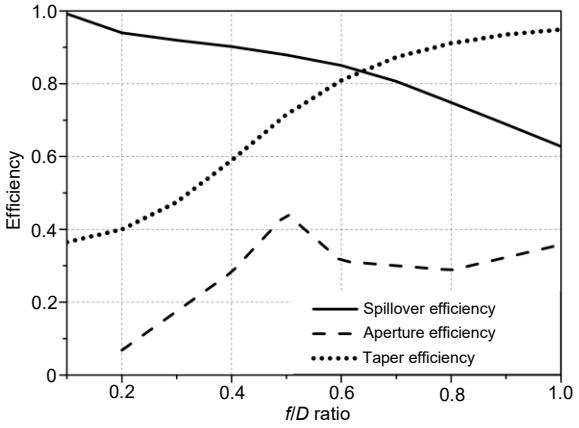

Fig. 10 Spillover, taper, and aperture efficiencies versus the *f*/*D* ratio

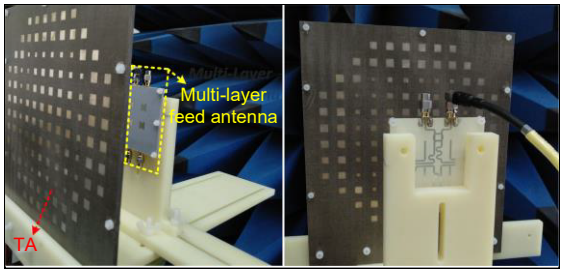

Fig. 11 Fabricated prototype of the monopulse transmitarray antenna (TA: transmitarray)

well. The 3-dB beam widths of the sum beam are 11° in both the E-plane and H-plane. The sidelobe level of the sum beam is below −13.4 dB. In addition, the cross-polarization level is below −20 dB. The measured gain of the sum beam is 21.5 dBi, which means that the calculated aperture efficiency is 32.2%.

Furthermore, the normalized far-field SUM-DIFF patterns from simulation (Sim.) and measurement (Mea.) are compared (Fig. 13). The gain ratios between the sum and difference beams are 7.56 dB and 4.7 dB in the E-plane and H-plane, respectively. We can improve the gain ratio performance of the monopulse

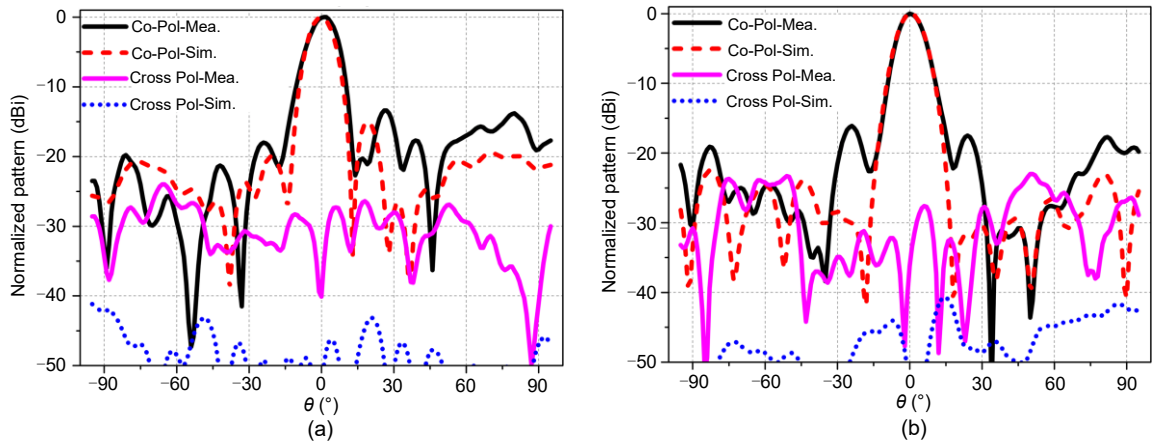

Fig. 12 Co-polarized (Pol) and cross-polarized sum pattern comparison between simulation (Sim.) and measurement (Mea.) in the E-plane (a) and H-plane (b)

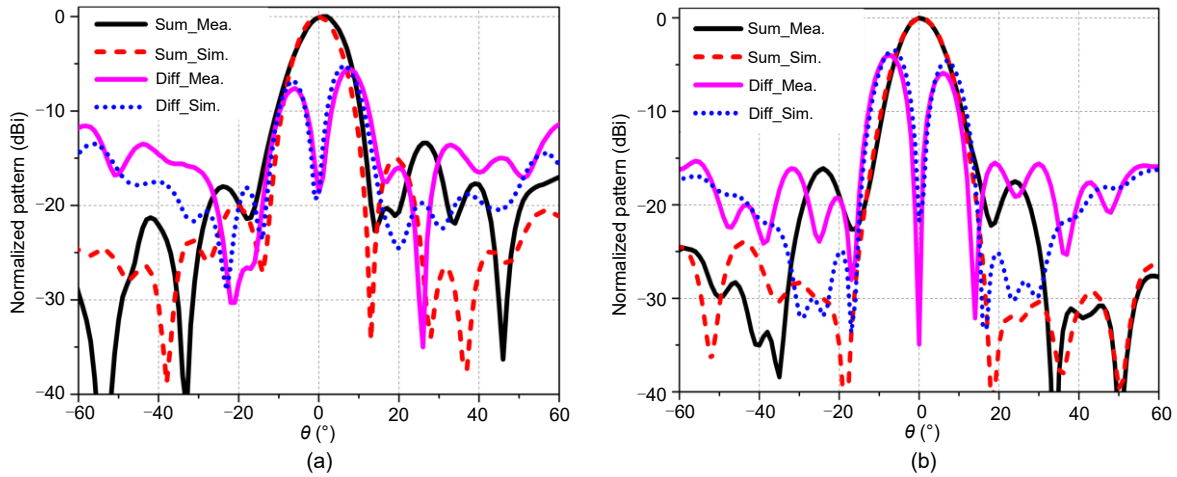

Fig. 13 Normalized far-field sum-difference (Sum-Diff) patterns in simulation (Sim.) and measurement (Mea.) in the E-plane (a) and H-plane (b)

transmitarray antenna by enlarging the size of the transmitarray. This can be used to increase the gain of the difference beam, thus reducing the discrepancy in gain between the sum and difference beams. The null depth of the difference beam is −18.6 dB in the E-plane and −34.9 dB in the H-plane. The null width (the angle between the two peaks of the difference pattern) is 13° in both the E-plane and H-plane. However, the results from simulation and measurement indicate that the measured sidelobe levels and cross-polarized patterns are both higher than the simulated ones. This might be caused by manufacturing errors, installation errors, or the reflection wave of the support structures. Figs. 14 and 15 show the E-field intensity and phase distribution maps of the ACMA at a distance of 100 mm, where the transmitarray is placed. Taking the DIFF2 feeding port as an example, the half area along the negative X axis is obviously a discontinuous area compared to that in Fig. 15a, when the SUM port is excited. When we calculate the compensated phase-shift distribution on the transmitarray, the reference

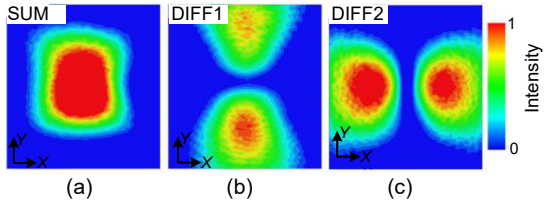

Fig. 14 E-field intensity distributions of the feed antenna at a distance of 100 mm when the SUM (a), DIFF1 (b), and DIFF2 (c) ports are excited (the size of the observation plane is 240 mm×240 mm)

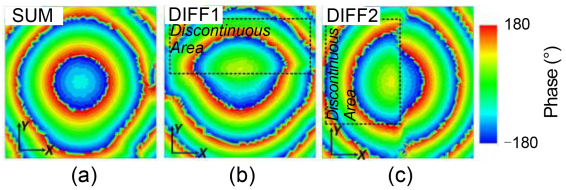

Fig. 15 E-field phase distributions of the feed antenna at a distance of 100 mm when the SUM (a), DIFF1 (b), and DIFF2 (c) ports are excited (the size of the observation plane is 240 mm×240 mm)

phase distribution should be as shown in Fig. 15a. Hence, the discontinuous phase distribution of feeding the DIFF2 port will result in gain loss of the far-field pattern in the corresponding angle. This further leads to the asymmetry of difference beams of the transmitarray antenna in both the E-plane and H-plane.

Since all the subassemblies are based on microstrip structures, the cost, weight, and dimensions of the proposed monopulse transmitarray antenna are greatly reduced. Table 2 shows the comparisons with existing comparable monopulse antenna designs. The first three designs adopt a microstrip antenna array fed by a microstrip comparator. The performance of monopulse microstrip antenna arrays is stable compared to that of the last three antennas. However, since the number of antenna elements in the microstrip array is large, the structure of the microstrip comparator is complex. The last three designs in Table 2 have a feed antenna with a reflectarray or transmitarray, whose feed comparator is simple. Among the three designs, ours has the highest aperture efficiency. Other reflectarray and

Table 2 Performance comparisons

Reference	Operating frequency (GHz)	Antenna form	SLL (dB)	Aperture efficiency (%)	Null depth (dB)	Peak gain (dBi)	Dimension (mm)
Yu et al., 2009	5.5–6.75	MS antenna array+MS comparator	−10	NA	−28	18.4	210
Kumar and Kumar, 2018	8.6–10.6	MS antenna array+MS comparator	−15	NA	−35	24.4	240
Wang et al., 2006	13.85–15.1	MS antenna array+MS comparator	−17	NA	−30	24.5	280
Zhao et al., 2018	35	Horn+SIW comparator+reflectarray	−12	22.4	−30	29.4	170
di Palma et al., 2016	10	Horn antennas+transmitarray	−14.4	16.6	−22.7	23.2	300
This work	10	Multi-layer MS antenna+transmitarray	−13.4	32.2	−18.6	21.5	200

MS: microstrip; SLL: sidelobe level; SIW: substrate integrated waveguide; NA: not applicable

reconfigurable transmitarray-based monopulse antennas use horn antennas as the feed source. In contrast, we use a multi-layer microstrip antenna as the feed source, whose feed network is relatively simple and has features such as light weight, low cost, and easy fabrication.

4 Conclusions

An X-band monopulse antenna based on a transmitarray is proposed in this paper. The combination of ACMAs and a sum-difference comparator is introduced as feed of the two-layered transmitarray, generating high-gain sum-difference patterns. Results from simulation and measurement showed good agreement. Sum beams with a 3-dB beam width of 11° and a sidelobe level of less than −13.4 dB were realized. Difference beams with gain ratios to sum beam of 5.6 dB in the E-plane and 4 dB in the H-plane were generated. The proposed transmitarray-based monopulse antenna has light weight, low cost, low profile, and easy fabrication features.

Contributors

Na KOU and Shixing YU designed the research, processed the data, and drafted the paper. Zhao DING and Zhengping ZHANG helped organize the paper. Na KOU and Shixing YU revised and finalized the paper.

Compliance with ethics guidelines

Na KOU, Shixing YU, Zhao DING, and Zhengping ZHANG declare that they have no conflict of interest.

References

Abdelrahman AH, Yang F, Elsherbeni AZ, et al., 2017. Analysis and design of transmitarray antennas. *Synth Lect Antenn*, 6(1):1-175. https://doi.org/10.2200/S00749ED1V01Y201612ANT012

Cao FF, Yang DQ, Pan J, et al., 2017. A compact single-layer substrate-integrated waveguide (SIW) monopulse slot antenna array. *IEEE Antenn Wirel Propag Lett*, 16:2755-2758. https://doi.org/10.1109/LAWP.2017.2744668

Didouh S, Abri M, Bendimerad FT, 2012. Corporate-feed multilayer bow-tie antenna array design using a simple transmission line model. *Modell Simul Eng*, 2012:327901. https://doi.org/10.1155/2012/327901

di Palma L, Clemente A, Dussopt L, et al., 2016. Radiation pattern synthesis for monopulse radar applications with a reconfigurable transmitarray antenna. *IEEE Trans Antenn Propag*, 64(9):4148-4154. https://doi.org/10.1109/TAP.2016.2586491

Kou PF, Cheng YJ, 2019. A dual circular-polarized extremely thin monopulse feeder at W-band for prime focus reflector antenna. *IEEE Antenn Wirel Propag Lett*, 18(2): 231-235. https://doi.org/10.1109/LAWP.2018.2886905

Kumar H, Kumar G, 2018. Broadband monopulse microstrip antenna array for X-band monopulse tracking. *IET Microw Antenn Propag*, 12(13):2109-2114. https://doi.org/10.1049/iet-map.2018.5332

Liu Y, Yang H, Jin ZS, et al., 2019. Multi-beam monopulse substrate integrated waveguide slot array antenna. *IET Microw Antenn Propag*, 13(2):142-148. https://doi.org/10.1049/iet-map.2018.5567

Lo KW, 1999. Theoretical analysis of the sequential lobing technique. *IEEE Trans Aerosp Electr Syst*, 35(1):282-293. https://doi.org/10.1109/7.745698

Poveda-García M, Cañete-Rebenaque D, Gómez-Tornero JL, 2019. Frequency-scanned monopulse pattern synthesis using leaky-wave antennas for enhanced power-based direction-of-arrival estimation. *IEEE Trans Antenn Propag*, 67(11):7071-7086. https://doi.org/10.1109/TAP.2019.2925970

Raman S, Barker NS, Rebeiz GM, 1998. A W-band dielectric-lens-based integrated monopulse radar receiver. *IEEE Trans Microw Theory Techn*, 46(12):2308-2316. https://doi.org/10.1109/22.739216

Roy SS, Saha C, Nagasekhar T, et al., 2019. Design of a compact multielement monopulse feed for ground-station satellite tracking applications. *IEEE Antenn Wirel Propag*

Lett, 18(9):1721-1725.
https://doi.org/10.1109/LAWP.2019.2927236

Sherman SM, Barton DK, 2011. Monopulse Principles and Techniques (2nd Ed.). Artech House, London, UK.

Vazquez-Roy JL, Tamayo-Domínguez A, Rajo-Iglesias E, et al., 2019. Radial line slot antenna design with groove gap waveguide feed for monopulse radar systems. *IEEE Trans Antenn Propag*, 67(10):6317-6324.
https://doi.org/10.1109/TAP.2019.2922742

Vosoogh A, Haddadi A, Zaman AU, et al., 2018. W-band low-profile monopulse slot array antenna based on gap waveguide corporate-feed network. *IEEE Trans Antenn Propag*, 66(12):6997-7009.
https://doi.org/10.1109/TAP.2018.2874427

Wang H, Fang DG, Chen XG, 2006. A compact single layer monopulse microstrip antenna array. *IEEE Trans Antenn Propag*, 54(2):503-509.
https://doi.org/10.1109/TAP.2005.863103

Yang TM, Zhao ZQ, Yang DQ, et al., 2019. A single-layer SIW slots array monopulse antenna excited by a dual-mode resonator. *IEEE Access*, 7:131282-131288.
https://doi.org/10.1109/ACCESS.2019.2940635

Yu ZW, Wang GM, Zhang CX, 2009. A broadband planar monopulse antenna array of C-band. *IEEE Antenn Wirel Propag Lett*, 8:1325-1328.
https://doi.org/10.1109/LAWP.2009.2038077

Zhao JN, Li TM, Cui XH, et al., 2017. A low-mutual coupling dual-band dual-reflectarray antenna with the potentiality of arbitrary polarizations. *IEEE Antenn Wirel Propag Lett*, 16:3224-3227.
https://doi.org/10.1109/LAWP.2017.2771205

Zhao JN, Li H, Yang XG, et al., 2018. A compact Ka-band monopulse cassegrain antenna based on reflectarray elements. *IEEE Antenn Wirel Propag Lett*, 17(2):193-196.
https://doi.org/10.1109/LAWP.2017.2779789

Zheng P, Zhao GQ, Xu SH, et al., 2016. Design of a W-band full-polarization monopulse cassegrain antenna. *IEEE Antenn Wirel Propag Lett*, 16:99-103.
https://doi.org/10.1109/LAWP.2016.2558285

Zheng P, Hu B, Xu SH, et al., 2017. A W-band high-aperture-efficiency multipolarized monopulse cassegrain antenna fed by phased microstrip patch quad. *IEEE Antenn Wirel Propag Lett*, 16:1609-1613.
https://doi.org/10.1109/LAWP.2017.2653840

Zhu JF, Liao SW, Li SF, et al., 2018. 60 GHz substrate-integrated waveguide-based monopulse slot antenna arrays. *IEEE Trans Antenn Propag*, 66(9):4860-4865.
https://doi.org/10.1109/TAP.2018.2847324